Three-dimensional structure of the human class II histocompatibility antigen HLA-DR1

Jerry H. Brown*, Theodore S. Jardetzky, Joan C. Gorga†, Lawrence J. Stern*, Robert G. Urban, Jack L. Strominger & Don C. Wiley*‡

Department of Biochemistry and Molecular Biology, * Howard Hughes Medical Institute, Harvard University, 7 Divinity Avenue, Cambridge, Massachusetts 02138, USA
† Department of Pediatrics, Children's Hospital of Pittsburgh, 6130 Rangos Research Building, 3705 Fifth Avenue, Pittsburgh, Pennsylvania 15213, USA

The three-dimensional structure of the class II histocompatibility glycoprotein HLA-DR1 from human B-cell membranes has been determined by X-ray crystallography and is similar to that of class I HLA. Peptides are bound in an extended conformation that projects from both ends of an 'open-ended' antigen-binding groove. A prominent non-polar pocket into which an 'anchoring' peptide side chain fits is near one end of the binding groove. A dimer of the class II $\alpha\beta$ heterodimers is seen in the crystal forms of HLA-DR1, suggesting class II HLA dimerization as a mechanism for initiating the cytoplasmic signalling events in T-cell activation.

Class II human leukocyte antigens (HLA) are cell surface $\alpha\beta$ heterodimers ($M_r \sim 60{,}000$) expressed primarily by specialized antigen-presenting cells such as macrophages, dendritic cells and B lymphocytes. Class II HLA presents peptides derived from extracellular antigens (refs 1, 2 but see refs 3, 4) to helper T cells as part of the mechanism for identifying foreign antigens and producing an immune response.

Class II HLA is polymorphic in the human population[5] and different types selectively bind different sets of peptides[1-3]. The HLA polymorphism appears to be responsible for variations in the immune response of different individuals to different antigens, and may contribute to the susceptibility to disease and autoimmune disorders[6,7].

Crystals have been grown from a number of class II HLA-DR (ref. 8) allelic variants after purification by immunoaffinity chromatography in detergent complexes and removal of the transmembrane region and cytoplasmic domain by papain digestion[9] and from a soluble construct of HLA-DR1 expressed in insect cells[10].

The three-dimensional structure of the extracellular portion of HLA-DR1 (DRA/DRB1*0101) has now been determined using three different crystal forms. In each crystal form, DR1 crystallizes as a dimer of the DR1 $\alpha\beta$ heterodimer. The class II structure is similar to that of the class I HLA molecule[11] and to a hypothetical model of the class II binding site based on the class I structure[12]. Structural differences from class I HLA include an altered position of the immunoglobulin-like β_2 domain of HLA-DR1 relative to that of the α_3 domain of class I HLA, and detailed changes in the peptide binding site so that its ends are more open. The peptide-binding site observed in the crystal structure contains electron density from the collection of peptides copurified with DR1 from human lymphoblastoid cells[4]. These peptides are bound as straight, extended chains that project out of both ends of the site. At one position of the peptide a side chain extends into a distinct pocket in the binding site. The main chain of the bound peptide contacts conserved, hydrogen-bonding residues along the HLA helices.

The presence of a parallel dimer of the $\alpha\beta$ heterodimers in crystals suggests the capacity of class II HLA molecules to dimerize before, or more probably during, recognition by helper T cells. Such a dimer of dimers could lead to an increased affinity for the CD4 coreceptor and to the crosslinking of T cell receptors to initiate cytoplasmic signalling pathways.

Structure determination

The three-dimensional structure of the extracellular portion of DR1 was determined to 3.3 Å resolution by combining X-ray diffraction data from three different types of crystals containing DR1: (1) Papain cleaved DR1 from human B lymphoblastoid cells carrying a mixture of endogenous peptides[8,9]; (2) the same DR1-peptide complex plus the 28K superantigen *Staphylococcus aureus* enterotoxin B (T.S.J. *et al.*, unpublished results); and (3) a complex of soluble DR1 expressed in insect cells with an antigenic peptide from the influenza virus haemagglutinin, HA 306-318 (ref. 10) (Table 1 legend).

An initial model of the polypeptide chain was determined from

‡ To whom correspondence should be addressed.

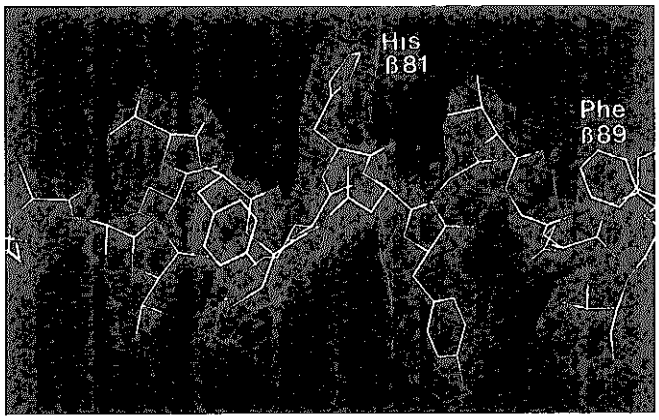

FIG. 1 Sixfold iteratively averaged 3.3 Å 'omit' electron density of the $\beta 1$ domain helix. About 83% of the polypeptide side chains show electron density of similar quality. Residues α 38, 46, 47, 50, 57, 126 and β 59, 64, 189 show no side-chain electron density, whereas residues α 1, 51, 52, 53, 132, 143, 181, β 42, 66, 68, 69, 70, 71, 72, 94, 108, 144 presently have ambiguous electron density.

an electron density map at 4.2 Å resolution, using phases from a single isomorphous heavy-atom derivative (0.12 mM K_2HgI_4, 0.3 mM KI) and iterative, fourfold, real-space averaging[13] of the first two crystal forms. Fourfold averaging was possible because each of the two crystals contained two crystallographically independent copies of the α-β heterodimer related by a non-crystallographic 2-fold symmetry axis (the symmetry axis in the dimer of heterodimers, Fig. 5*a*). Phases were improved by model building and iterative sixfold real-space averaging about the non-crystallographic 2-fold symmetry axes of all three crystal forms. Real-space averaged 'omit'[14] maps, now at 3.3 Å resolution, show excellent density for 83% of the polypeptide side chains (Fig. 1). Nine side chains show no electron density. Seventeen residues have ambiguous electron density, including β-chain residues 68–72 which have been provisionally modelled as helical. Though electron density is observed to emanate from each of the three oligosaccharide attachment sites (most extensively at α 118), it has not yet been interpreted as a molecular model. Refinement of DR1 in the three crystal forms is in progress.

Structural comparison with class I HLA

Overall the structure of DR1 is similar to that of class I HLA (Fig. 2*a*). The two α-chain domains, α_1 and α_2, of DR1 superimpose closely on the corresponding α_1 domain and the β_2-microglobulin subunit, respectively, of class I HLA. The two β-chain domains, β_1 and β_2, of DR1 superimpose on the α_2 and less closely on the α_3 domains, respectively, of class I HLA. The β_2 domain of DR1 is offset relative to the HLA-A2, class I α_3 domain by about 15° (Fig. 2*a*), but the packing between the class II immunoglobulin domains still resembles the packing in class I more than the packing in an antibody.

The peptide-binding groove of both class I and class II HLA is composed of eight strands of antiparallel β-sheet as a floor and two antiparallel helical regions as the sides. The similarity between the two structures extends even to the location of β-bulges in the β-strands and the locations of kinks in the helices (Fig. 2*b*). With the exception of the sequence alignment in strand 4 (residues α 37 to α 43) of the α_1 domain, a hypothetical model of class II (ref. 12) based on the class I HLA-A2 structure is correct. (A number of segments deemed unpredicable based on sequences and the class I structure have a different structure in class II antigens.)

Differences in the helical regions of class II HLA relative to class I may determine why class I HLA binds primarily short, nonameric peptides[15], whereas class II HLA binds longer, 15-

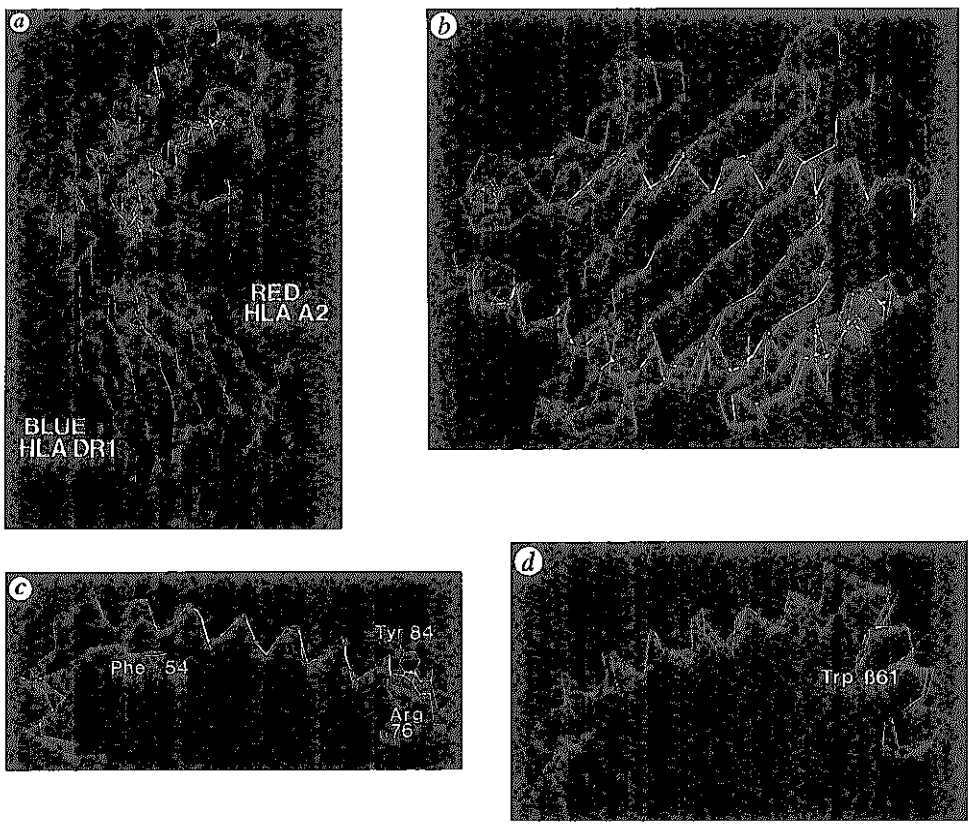

FIG. 2 Class II HLA-DR1 (blue) superimposed on class I HLA-A2 (red). *a*, One DR1 $\alpha\beta$ heterodimer and one HLA-A2 molecule[34]. The β_2 DR1 domain is offset from its homologue the α_3 HLA-A2 domain by about 15°. *b*, 'Top' view shows the overall similarity of the peptide binding sites. HLA-A2 α_1 and DR1 α_1 domains' helices are at the top, those of HLA-A2 α_2 and DR1 β_1 are at the bottom. *c*, 'Side' view of α_1 domain helical regions showing differences at both ends. On the left (also seen in *b*) DR1 has an extended chain where the HLA-A2 has helical residues. On the right, DR1 is about 2.0 Å lower (at Arg α76) than HLA-A2 Tyr 84. *d*, 'Side' view of the helical regions of the DR1 β_1 and HLA-A2 α_2 domains. DR1 has a more prominent kink and Trp β 61 superimposes almost exactly on HLA-A2 Trp 147. α-Carbon coordinates were superimposed by the program FITATOM (W. Kabsch) based on the central six β strands and two long helices of the peptide-binding site.

24 residue, peptides[1-4]. Two turns near the amino terminus of the class I α_1 domain helical region are replaced by a stretch of extended chain in class II (Fig. 2*b*, *c*). The carboxy-terminal end (right, Fig. 2*c*) of the class II α_1 helical region bends more towards the floor of the site such that arginine, α 76, is 2.0 Å 'lower' in the site than the homologous class I residue tyrosine 84. These alterations help 'open' the peptide-binding site of class II HLA, so that long peptides can be accommodated. There is also a slightly more protuberant kink in the β_1 helical region of DR1 (right, Fig. 2*d*), as predicted[16], and this helical region ends (left, Fig. 2*d*) in an extended chain in DR1 rather than a kink and short helix as in class I HLA. The regions that differ in secondary structure between class I and class II also differ in their patterns of polymorphism, being relatively conserved in class I and relatively polymorphic in class II[12].

In addition to these differences in secondary structure between the class I and class II binding groove, a number of specific amino-acid side chains that 'close' the ends of the class I site are not present in the class II site. The conserved tyrosines (7, 59, 171) that bind the peptide N terminus and the conserved residues (Y84, K146, T143) that bind the peptide C terminus in the class I structure[17-19] are not found in class II sequences. Furthermore, a nearly conserved tryptophan (167) and salt bridge (Glu 55 to Arg 170) which 'close' the 'left' (Fig. 2) end of the class I groove[20] are absent in class II sequences. The significantly smaller side chain (glycine or valine) at β 86 compared to the class I homologue tyrosine 171 helps create a deep pocket in the DR1 groove surrounded by predominately non-polar residues of both the α_1 and β_1 domains (left in Fig. 3). This pocket, which provides the binding site for a peptide 'anchor' side chain in DR1, is composed of class II residues homologous to class I residues beyond the 'left' end of the class I binding groove.

Residues in the binding site

The distribution of conserved and polymorphic positions in the class II peptide-binding site suggests how conserved class II residues contact main chain atoms of bound peptides and where polymorphic pockets might bind the side chains of peptides. Figure 3 shows that three conserved asparagine residues, 62 and 69 in the α_1 helical region and 82 in the β_1 helical region are positioned such that their γ amide groups might hydrogen bond with the main-chain peptide atoms of bound peptides. Mutation of β 82 to serine affects intracellular transport and cell surface expression of murine class II molecules, consistent with this observation[21]. Conserved tryptophan β 61 is placed so that its indole nitrogen could donate a hydrogen bond to a main chain carbonyl group of a bound peptide in exact homology to the location and function of tryptophan 147 of class I HLA[17]. The orientations of the murine I-A^k equivalents of α_1 helical residues 57–75 were previously deduced from alanine scanning mutagenesis[22].

Several clusters of polymorphic residues, spaced across the binding site, appear to provide the mechanism by which different types of class II HLA selectively bind peptides of different sequences[23-26]. The first cluster (α 31, 52; β 86, 89, 90) appears to provide variability to a peptide side chain pocket composed

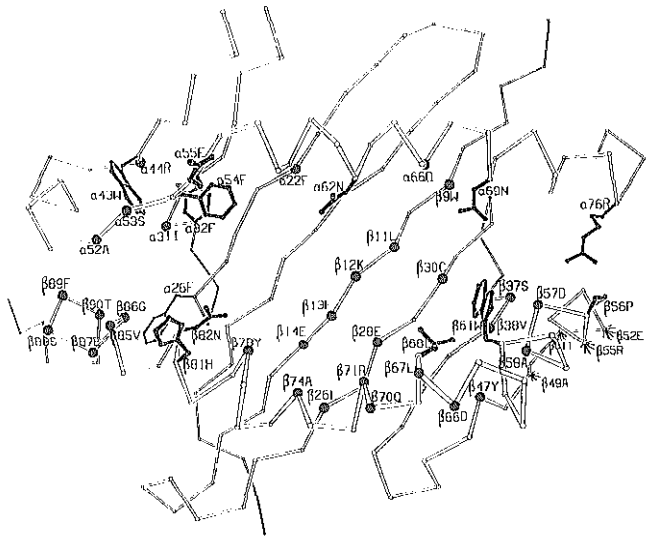

FIG. 3 The class II α_1 and β_1 domains, showing all polymorphic positions (dark circles, POL > 2[12]) and those conserved positions facing the antigen-binding groove (all atoms of side chain shown). Amino-acid residues, in one letter code, and positions are given for DR1 (DRA/DRB1*0101). The antigen-binding groove of DR1 includes the side chains of residues 7, 9, 11, 22, 24, 26, 31, 32, 43, 51, 53, 54, 55, 58, 62, 65, 68, 69, 72, and 76 of the α chain, and residues 9, 11, 13, 28, 30, 32, 37, 38, 47, 56, 60, 61, 65, 68, 70, 71, 74, 78, 81, 82, 85, 86, 88, and 89 of the β chain. Residues whose side chains are in the dimer interface (see text and Fig. 5) are indicated by 'starbursts'.

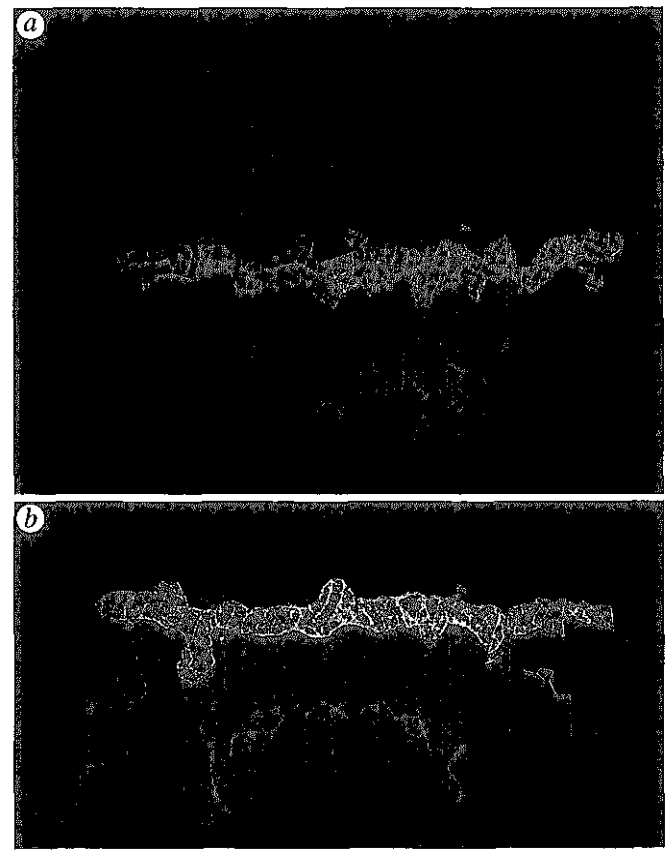

FIG. 4 Peptides bound to crystalline DR1 from human cells. Red, Electron density of the collection of endogenous bound peptides; Blue, van der Waals surface of DR1. *a*, 'Top' view, probably as seen by T cells; α_1 domain helix on top, β_1 domain helix on bottom; peptide N terminus at left. An extended, 15 amino-acid long, α-carbon, peptide backbone is placed in the electron density for scale. The side chains shown at the right-hand end of the site are arginine α76 and aspartic acid β 57 which form a salt bridge under the exiting peptide. *b*, 'Side' view, β_1 domain helix removed for clarity, β-sheet shown below and α_1 domain helix shown behind peptide electron density. The prominent downward facing peptide side chain electron density near the left end of the peptide is located about one peptide residue to the left of where the N terminus of peptides bound to class I HLA are positioned. Electron density map is fourfold iteratively averaged, 3.3 Å resolution, using DR1–LG2 and DR1–SEB crystal forms (see Table 1 legend) and $2F_o$–F_c coefficients. Density within 1.5 Å of provisional peptide atoms is included.

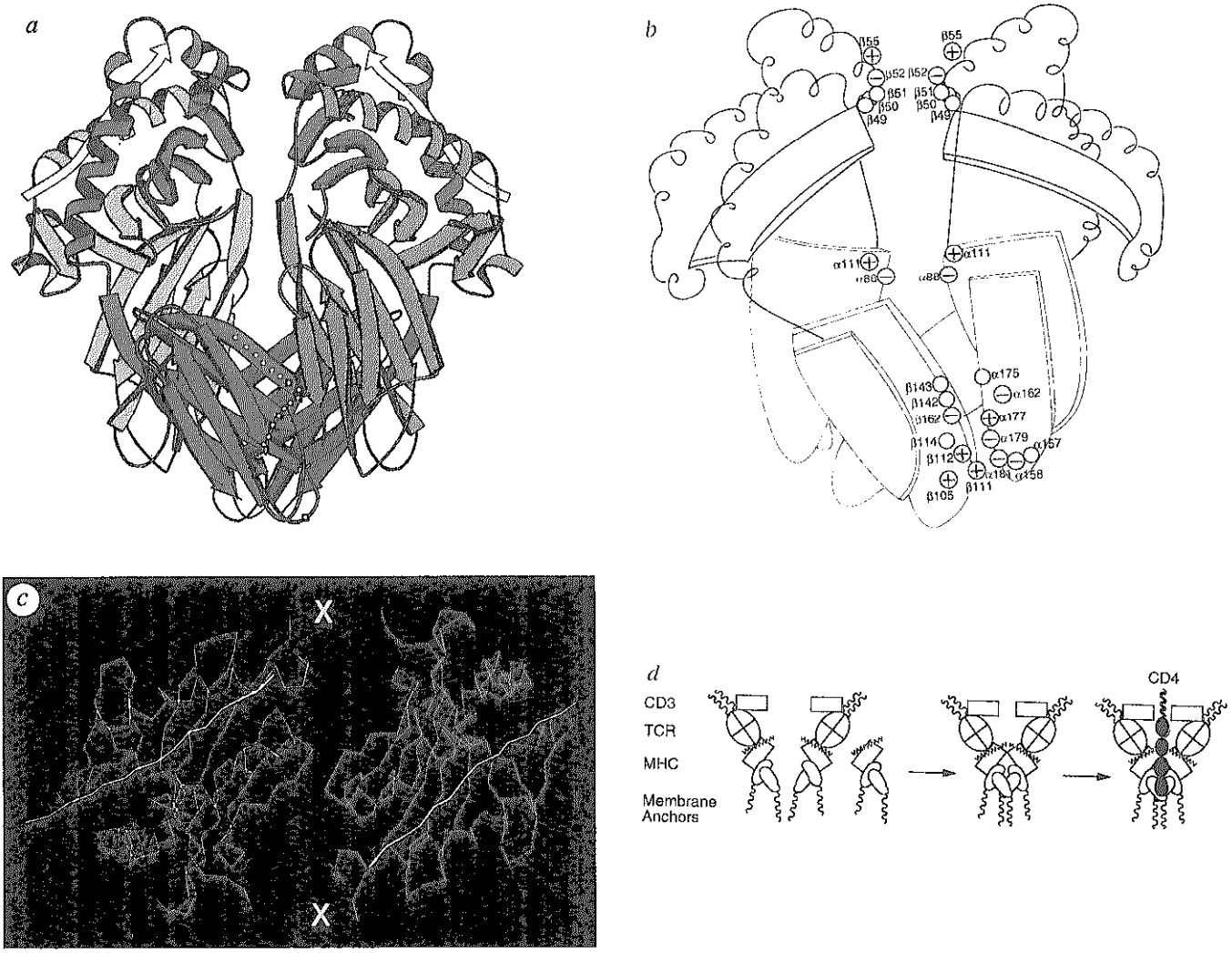

FIG. 5 DR1 crystallizes as a dimer of the $\alpha\beta$ heterodimer. *a*, One DR1 molecule is shaded in red, the other in blue, peptides are yellow. The α-chains are the lighter shades, the β-chains are darker. The width of the dimer shown is 76 Å; the height is 73 Å. β_2 residues implicated in CD4 binding by mutagenesis[40] (□), by peptide binding[41] (○). α_2 domain residues near the β_2 domain residues that have been implicated in CD4 binding are α 116, 118, 120, 122, 125, 127, 129, 164, 166, 168, 171, 172 and 173. *b*, Residues which make contact (<3.5 Å) in current, unrefined model across the DR1 dimer interfaces are indicated. Red, Asp or Glu; Blue, Arg, Lys, His. The second dimer-related interface at the bottom is not shown. A total of 1,293 Å^2 of one DR1 heterodimers solvent accessible surface is buried by the other, larger than the interface between antibody and protein antigen[68]. Surface areas in DR1 were obtained using ACCESS with a probe radius of 1.4 Å (written by M. D. Handschumacher and F. M. Richards), and may slightly change upon refinement. *c*, The dimer of antigen-binding domains as seen from the top. The closest approach of the bound portions of the two peptides (in yellow) is ~30 Å, the furthest distance being about 80 Å. 'X' marks the probable locations of the CD4 coreceptors. *d*, Hypothetical assembly pathway for an antigen-specific, cell cell interaction complex of class II HLA, T-cell receptor, and the coreceptor CD4 (see text). Further aggregation may occur if CD4 dimerizes[69] (J. Wang and S. C. Harrison, personal communication). (An alternative model where CD4 binds before TCR has similar properties but is less consistent with CD4-independent T-cell recognition.) The box marked CD3 is intended to symbolize the CD3, ζ, and associated components of the T-cell receptor.

of mostly conserved (α 26, 32, 43, 54) non-polar residues in class II HLA (Fig. 3). Three other polymorphic clusters are found at three, five and about seven or eight residues further along the bound peptide, composed of β 13, 26, 28, 71, 74, 78; α 66, β 9, 11, 30 and β 37, 38, 58. The clustering of the murine I-E and I-A equivalents of β 71 and β 74 with β 28 has previously been suggested from mutual compensatory effects of mutations at those residues on peptide binding and T cell response[27]. The structure is also consistent with earlier observations of the effect of allelic specific residues on α–β chain pairing[28,29].

The polymorphic residue aspartic acid β 57 in DR1 appears to form a salt bridge with a conserved arginine α 76 (Fig. 3) under the exiting peptide (see below). Aspartic acid β 57 in the HLA-DQ isotype has been found to correlate with protection against insulin-dependent diabetes mellitus (IDDM) in humans, as HLA-DQ allelic products with side chains of β 57 incapable of forming a salt bridge are linked to susceptibility to IDDM[7,30]. In the non-obese diabetic mouse alterations at β 57 in I A^k have been implicated in insulitis[31–33], but other genes also appear to be involved in generating disease[31]. In addition to a possible effect on peptide binding, polymorphism at β 57 may affect the stability or structure of the dimer of $\alpha\beta$ heterodimers because nearby residues β 52 and β 55 form part of the interface of the dimer (see below).

Structure of bound endogenous peptides

The electron density in the binding groove (Fig. 4), which represents the collection of endogenous peptides from human lymphoblastoid cells, is straight and thin as expected for a peptide in an extended conformation. This density indicates that about

TABLE 1 Data collection statistics

X-ray Temp.	Protein (source)	Space group (Z*)	*a*, *b*, *c* (Å)	Deriv.	Resolution R_{merge} comp(red)†	Resolution R_{merge} comp(red)†	ΔF	r.m.s. f_h/E†
GX-13 4 °C	DR1(LG-2)	$C222_1$ (2)	96.7 112.6 209.2	native	100–4 Å 0.117 74% (1.5)	4.5–4.2 Å 0.222 60% (1.4)		
GX-13 4 °C	DR1(LG-2)	$C222_1$ (2)	96.6 112.6 209.2	K_2HgI_4	15–4.2 Å 0.099 73% (1.2)	4.4–4.2 Å 0.198 63% (1.1)	0.20 (15–4.2 Å)§	1.49
GX-13 −165 °C	DR1(LG-2) SEB‖	$P2_12_12_1$ (2)	95.7 115.9 150.4	native	30–3.4 Å 0.101 70% (1.44)	3.6–3.4 Å 0.24 51% (1.47)		
GX-13 −165 °C	DR1(LG-2) SEB‖	$P2_12_12_1$ (2)	95.9 117.1 150.8	K_2HgI_4	30–3.2 Å 0.077 83% (4.0)	3.4–3.2 Å 0.229 76% (2.23)	0.185 (30–3.5 Å)§	1.3
CHESS −170 °C	DR1(LG-2)	$C222_1$ (2)	96.7 114.4 216.8	native	15–2.7 Å 0.082 90% (2.4)	3.4–3.2 Å 0.168 95% (2.7)		
CHESS −170 °C	DR1(LG-2) SEB‖	$P2_12_12_1$ (2)	95.0 114.7 149.8	native	20–2.8 Å 0.057 88% (3.3)	3.0–2.8Å 0.224 89% (3.5)		
CHESS −170 °C	DR1(SF9) HA306–318	$P4_32_12$ (2)	95.4 95.4 245.7	native	20–2.7 Å 0.068 93% (3.2)	3.0–2.9 Å 0.221 94% (3.2)		

Averaging statistics

	4.2 Angstrom 4-fold		3.3 Angstrom 6-fold		
	DR1(LG-2)	DR1/SEB	DR1(LG-2)	DR1/SEB	DR1(SF9)
R§	0.23	0.23	0.31	0.30	0.30
Mean-phase Difference					
Overall	75.3°	68.7°	56.8°	67.5°	51.1°
Last cycle	2.8°	3.3°	3.2°	4.8°	3.1°

DR1 and a number of other subtypes and isotypes of human class II histocompatibility antigens have been crystallized[8] after purification by immunoaffinity chromatography in detergent complex and removal of the transmembrane region and cytoplasmic domain by papain digestion[9]. Crystals of DR1 isolated from the human B lymphoblastoid cell line LG-2 (DR1–LG2) suitable for high-resolution study were initially grown at pH 4.0 and later at pH 5.5–6.0 from 27% PEG 8000, 0.1 M glycine, 0.01% NaN_3, 0.05 M MES. Crystals of the superantigen SEB in 1:1 complex with DR1–LG2 were grown using the same human-cell derived DR1 mixed with SEB (Sigma) further purified by gel filtration and will be described further elsewhere (T.S.J. *et al.*, manuscript in preparation). DR1 expressed as a soluble heterodimer in SF9 insect cells (DR1–SF9), purified as an empty molecule, and subsequently complexed with the influenza virus 13-mer peptide HA 306–318 crystallized from 15% PEG 8000, 0.02% NaN_3, 100 mM sodium acetate, pH 4.6[10]. Crystals of DR1–LG2 and the DR1–SEB complex were soaked overnight in 0.12 mM K_2HgI_4, 0.3 mM KI. Native and derivative X-ray data (first four sets of rows) were collected with a Xentronics area detector using an Elliot GX-13 X-ray source focused with Franks mirrors[62], then integrated and scaled using the BUDDHA[63] and CCP4 packages. Two heavy-atom positions per asymmetric unit were found to be 27.5 Å apart by analysis of difference Patterson maps of both crystals. Electron density maps were calculated at 6 Å resolution using single isomorphous replacement (SIR) phases for DR1–LG2 and SIR with anomalous scattering for DR1–SEB. A relationship between the electron density in the two crystal forms was found by a one-dimensional, real-space correlation search along the Hg to Hg vector in the two crystals using the program CYLINDER (written by P. Metcalf). The maps from the two crystals were then averaged. An envelope could be constructed around the DR1 portion of the electron density from the average map, and the remaining electron density in the DR1–SEB crystals was assigned to an SEB envelope. Thirteen cycles of iterative, real-space averaging within the DR1 envelopes and solvent flattening outside of DR1 and DR1–SEB in the two crystal forms were done using CCP4 and Joy of skewing[13]. Input for the first cycle of averaging include observed structure factors (F_{obs}) and single isomorphous replacement phases (ϕSIR) for DR1–LG2 and F_{obs} and ϕSIR/anomalous for DR1–SEB. Input for cycles 2→4 include F_{obs} and combined phases (ϕcomb)[13]. Input for cycles 5→8 included combined structure factors (F_{comb})[64] and ϕcomb. Input for the final 5 cycles included Sim-weighted $2F_{obs}-F_{calculated}$ coefficients and calculated phases. This procedure yielded an electron density map from which the domain structure was evident for two, $\alpha\beta$ heterodimers of DR1 per asymmetric unit in each crystal. Using the 2-fold noncrystallographic rotational symmetry within each crystal's asymmetric unit, the above averaging procedure was repeated, but now real-space averaged 4-fold within the DR1 envelopes, 2-fold within the SEB envelopes, and solvent flattened outside the envelopes at 4.2 Å resolution (left side of averaging statistics). The DR1 polypeptide pathway and many large side chains were evident at this point. The Hg derivative was seen to label the only free cysteine (β 30). Higher resolution, more complete X-ray data were then collected on phosphor image plates at CHESS (and integrated using DENZO (Zbyszek Otwinowski, personal communication)) from crystals that had been soaked in cryoprotectant (row sets 5–7) and mounted in nichrome (DR1–SEB) or glass (DR1–LG2 and DR1–SF9) loops[65] and flash frozen to −165 °C in a stream of cold nitrogen. A partially refined model of DR1 (against synchrotron-cryo DR1–LG2) was fit and refined as rigid domains using X-PLOR version 2.1 (written by A. Brünger) into the 3 or 3.5 Å resolution cryo-X-ray data of the other two crystals. For each of the three crystal forms, eight 'omit models' were constructed[14], each missing about one-eighth of the DR1 model. The DR1–LG2 'omit' models were subjected to a simulated annealing refinement procedure to reduce bias[66]. 'Omit maps' were calculated from each 'omit' model. Eight cycles of sixfold, iterative, real-space averaging of the electron density within the DR1 envelopes of both monomers in the 'omit' maps of all three crystals (right side of averaging statistics) yielded the current 3.3 Å (Fig. 1) map. A model has been built using FRODO[67].

* Z, Number of DR1 heterodimers per asymmetric unit.

† Comp, % completeness = 100 × (number of independent reflections)/(maximum number theoretical), red, redundancy = (number of measurements)/(number of independent reflections). CHESS = Cornell High Energy Synchrotron Source, GX-13 = Elliot rotating anode.

‡ f_h, Heavy-atom structure factor; E the residual lack of closure.

§ Resolution range used for heavy-atom derivative statistics, ΔF and r.m.s. f_h/E.

$$R_{Morgo} = \frac{\sum_{hkl}\sum_{obs}|I^{hkl}_{obs} - \langle I^{hkl}\rangle|}{\sum_{hkl}\sum_{obs} I^{hkl}_{obs}}, \qquad \Delta F = \frac{\sum_{hkl}|F_{native} - F_{derivative}|}{\sum_{hkl} F_{native}}, \qquad R = \frac{\sum_{hkl}|F_{observed} - F_{calculated\ from\ average\ map}|}{\sum_{hkl} F_{observed}}$$

‖ SEB source: SEB used in these frozen crystals was a gift from M. Sax, VA Medical Center, Pittsburgh, PA. The same crystals were also obtained from SEB purchased from Toxin Technology Inc., Sigma, or purified from an SEB producing strain of *S. aureus*.

15 peptide residues contact HLA-DR, consistent with the average length of the most abundant peptides bound to DR1 from LG2 cells[4]. The electron density is not weak in the middle as observed in class I HLA-A2[34] and HLA-Aw68[35] (but not HLA-B27[17]) where peptides of different length appear to be accommodated by bulging out of the site near the middle[17,19,35]. Instead it extends out of both ends of the site, consistent with the observation that the endogenous peptides of class II HLA vary in length from 12–24 amino acids and have 'ragged' ends[1,4].

The current DR1 model is based on averaging the 3.3 Å resolution data of different crystal types and is not crystallographically refined, so no detailed model for the bound peptides has been constructed. (A more complete analysis of peptide contacts is in preparation at higher resolution for the complex between DR1 and influenza virus haemagglutinin peptide, HA 306-318 (L.J.S. *et al.*, unpublished data). But the electron density from LG2 cell-derived DR1 (Fig. 4*b*, left end) indicates the position of one prominent peptide side chain that appears bound in a hydrophobic pocket near residues α 26, 31 and β 86. This seems to be the position of the dominant 'anchoring' peptide residue predicted at position 308 of the influenza HA (306–318) peptide both by binding studies of substituted peptide sequences and by the high-affinity binding of a simplified peptide where all but two residues were made alanine[36]. The size of this peptide residue side chain seems to parallel the size of the non-polar pocket as modulated by the Gly–Val dimorphism at β 86[37,39]. These observations and the homologous role observed for tryptophan β 61 in class II and tryptophan 147 in class I (see above) suggest that peptides are bound with their N termini to the left (in Fig. 3), an orientation homologous to that in class I sites. This has been confirmed for one peptide HA306–318 complexed with HLA-DR1, which is currently being refined to 2.7 Å resolution (L.J.S. *et al.*, unpublished data). The clarity of the peptide electron density may in part be due to the predominance of a few peptides in DR1 from LG2 cells[4].

A dimer of $\alpha\beta$ heterodimers

Because a dimer (Fig. 5*a*) is observed in DR1 crystals, it may represent an intrinsic property of DR1 (see next section). There are four interfaces between DR1 molecules in the dimer (Fig. 5*b*). Two small interfaces are near the 2-fold rotational symmetry axis that relates the molecules (top two in Fig. 5*b*), β_1 49–55 and α_2 88, 111. In the most membrane-distal interface, five β_1 domain residues of one molecule contact the same residues in the β_1 domain of the second molecule, burying 305 Å^2 of solvent accessible surface on each monomer (see also Fig. 3). Four of these residues are conserved in all DR alleles. Two salt bridges from glutamic acid β 52 to arginine β 55 on the other molecule are conserved in DR, but are replaced by proline and leucine residues in some DP and DQ variants. The second interface is simply two salt bridges between glutamic acid 88 and lysine 111 of the second domain of the conserved DR1 α chain. This interface is small, burying 75 Å^2 of surface per monomer.

The bottom two interfaces are identical and are located about 12 Å from the dimer rotation axis at the membrane proximal end of the dimer (Fig. 5*b*). Each is composed of 7 residues on the β_2 domain of one molecule in contact with 7 residues on the α_2 domain of the other molecule and buries surfaces of about 900 Å^2. Most of the residues are conserved in class II HLA sequences including those participating in three salt bridges between α_2 domain residues glutamic acid 158, histidine 177, glutamic acid 179 and β_2 domain residues histidine 111, glutamic acid 162 and histidine 112.

CD4 binding site

The T-cell coreceptor molecule, CD4, is thought to bind to the β_2 domain of DR1 based on mutagenesis that indicated CD4 affinity changes when β_2 domain residues 110, 137, 140, 141 and 142 were altered[40] and based on the observation that peptides with the sequence of β_2 domain residues 134–148 (and less so, 138–152) could bind to CD4[41] (white symbols in Fig. 5*a*). If the DR1 dimer is present during T-cell recognition, the X-ray structure suggests that a region on the α_2 domain of the second DR1 molecule in the dimer (light blue domain near white symbols, Fig. 5*a*) might also contact CD4, potentially increasing the affinity of the DR1–CD4 interaction over that possible between CD4 and a single DR1 molecule. (α_2 domain positions near the β_2 CD4 site are listed in Fig. 5*a* legend.) Some of the β_2 domain positions identified by mutagenesis as important for CD4 binding are in (β 141, 142) or near (β 110 for which the affinity effect is only partial[40]) the dimer interface raising the possibility that some of the observed CD4 affiity changes may have been due to destabilization of a class II HLA dimer. Viewed from the 'top' (Fig. 5*c*), the DR1 dimer presents two peptide binding site surfaces presumably for recognition by T-cell receptors and two slots between them (X in Fig. 5*c*). The presumptive CD4-binding sites described above are located behind the Xs in Fig. 5*c*.

Conclusion

HLA class II versus class I peptide binding. The class II DR1 structure shows that the peptide-binding site is open at both ends (Fig. 4). Long peptides, at least 15 residues, are seen to be bound in an extended conformation, projecting out of both ends of the site. This contrasts with peptides bound to class I HLA molecules where mostly 9-mers bind with extended, but kinked, conformations, and the N and C termini of the peptides are sequestered in conserved, peptide-terminal binding sites[17,19,35]. In the mechanism by which MHC molecules bind many peptides tightly, the role of clusters of conserved residues in class I HLA binding of peptide termini[17,35,42] appears to be replaced in class II HLA by conserved residues (β82N, α62N, α69N, β61W, α76R) spaced so as to bind at intervals (Fig. 3) to the extended main chain of bound peptide, providing a peptide side chain independent component to the affinity.

In class I MHC molecules polymorphic residues in the binding site form pockets which accommodate peptide side chains and which form the basis for allele-specific peptide binding[17,19,34,35,43]. In class II DR1 one prominent peptide side chain at about the third position of a 15-mer identifies a critical binding pocket, and other pockets are inferred from the locations of polymorphic residues and the shape of the electron density representing multiple peptides complexed with DR1 (Figs 3 and 4). The critical binding pocket of DR1 lies near one end (left in Figs. 3 and 4) of the class II binding groove, before the location where the class I groove begins. The location of this critical pocket, the orientation of the peptide, and the extended conformation of the peptide are consistent with some of the previous studies of peptide interactions with class II proteins[36,44,45].

Possible implications of a class II HLA dimer of dimers. Two observations suggest that the dimer of DR1 $\alpha\beta$ heterodimers discovered in the three crystals studied is suitable for a physiological role. (1) In the dimer two DR1 molecules are parallel to each other so that all four C termini face one direction (down in Fig. 5*a*) and both peptide-binding sites face the opposite direction (up in Fig. 5*a*) as might be expected for glycoproteins on a membrane surface. (2) The two peptide-binding regions are oriented so that two molecules the size of the $\alpha\beta$ T-cell receptor could contact these binding sites simultaneously.

The possibility that the dimer is a crystallization artefact is not ruled out. It is also possible that a dimer stable only at high protein concentrations in solution has been stabilized by crystallization. Whether stabilization conditions might exist physiologically to take advantage of this capacity to form dimers is discussed below. Whether the dimer exists *in vivo* can be tested by site-directed mutagenesis. If the observed dimer of DR1 molecules is physiologically important, its structure suggests that mutations in the α_2 domain may affect CD4 binding (see Fig. 5*a* legend) and that mutations in the dimer interfaces (Fig. 5*b*) may affect both CD4 binding and T-cell activation.

The capacity of DR1 molecules to form a parallel dimer suggests the possibility that the observed dimerization might provide part of the mechanism for initiating intracellular signalling pathways both in T cells by crosslinking two T-cell receptors[46,47] and, in antigen presenting cells, to induce the expression of costimulating molecules[48–51]. Dimerization of cell-surface receptors with the concomitant dimerization of their cytoplasmic domains is an established mechanism for signal initiation in some hormone receptor interactions, for example that of human growth hormone[52]. Indeed, T-cell receptors can be activated by crosslinking with a divalent antibody but are not activated by the cognate monovalent Fab fragment[53]. But hydrodynamic and other measurements provide no evidence that DR1 dimerizes in solution[8,10,54] (although detergent-soluble DR1 migrates anomalously on gel filtration[55]), even at the acidic conditions (pH 4.0–6.0) used in crystallization (L.J.S., unpublished data).

Low affinity in the dimer interaction may be an important feature for T-cell activation. Unless a mechanism exists for loading both peptide-binding sites of a single dimer with the same peptide, dimers preexisting on antigen-presenting cells would be expected to contain two different peptides, only one being specific for a given T cell. Weakly interacting DR1 molecules would exchange more readily, allowing T-cell receptor recognition a role in the assembly of an activation complex.

If the T-cell receptor binds to monomeric DR1 molecules and affects dimerization, many mechanisms for initiating signalling can be generated. For one example (Fig. 5*d*), assume that the $\alpha\beta$ T-cell receptor (and its associated CD3 and ζ subunits) can also form weak dimers like those of DR1, then before DR1–TCR binding neither DR1 nor TCR dimers would be stable (Fig. 5*d*, left). Once DR1 molecules with a specific peptide are bound by a TCR, each such complex would be able to form a stable dimer by using both the weak dimerization sites of DR1 and of the TCR molecules simultaneously, achieving stability by a chelating effect (Fig. 5*d*, middle)[56]. The DR1 dimer structure further suggests that the affinity for the coreceptor CD4 could be greater after dimerization due to contacts with both monomers, suggesting both that adhesion contributed by CD4 would be increased after TCR-dependent dimer assembly, and that signalling through CD4[57] could be triggered by its association with this complex (Fig. 5*d*, right). Concentrations sufficient to drive the assembly process (Fig. 5*d*) may be found in the synapse-like contacts between T cells and their target cell.

Some peptides that bind to class II MHC but engage the T-cell receptor weakly or differently do not initiate full T-cell signalling and therefore act as pure antagonists or mixed agonist/antagonists[58–60]. Such MHC–TCR complexes might be expected to assemble into the interaction complex proposed above (Fig. 5*d*, right), but could destabilize it below the threshold required to stimulate complete intracellular signalling.

A synergistic, multisubunit assembly process, where each interaction increases the affinity of subsequent interactions, would have the potential to amplify an initially small, but specific, interaction between the $\alpha\beta$ chains of TCR and HLA into a stable, antigen-specific complex that bridges both sides of the T-cell membrane and the antigen-presenting cell membrane (Fig. 5*d*, right). This mechanism substitutes direct, stable molecular contacts to initiate full intracellular signalling for previous models that invoked statistical increases in the local density of TCR–HLA complexes to lead to T-cell activation[47,61]. □

1. Rudensky, A. Y., Preston-Hurlburt, P., Hong, S.-C., Barlow, A. & Janeway, C. A. Jr *Nature* **353,** 622–626 (1991).
2. Hunt, D. F. *et al. Science* **256,** 1817–1820 (1992).
3. Chicz, R. M. *et al. J. exp. Med.* **176,** 27–47 (1993).
4. Chicz, R. M. *et al. Nature* **358,** 764–768 (1992).
5. Kappes, D. & Strominger, J. L. *A. Rev. Biochem.* **57,** 991–1028 (1988).
6. Tiwari, J. L. & Terasaki, P. I. *HLA and Disease Associations* (Springer, New York, 1985).
7. Todd, J. A. *et al. Science* **240,** 1003–1009 (1988).
8. Gorga, J. C., Brown, J. H., Jardetzky, T., Wiley, D. C. & Strominger, J. L. *Res. Immun.* **142,** 401–407 (1991).
9. Gorga, J. C., Horejsi, V., Johnson, D. R., Raghupathy, R. & Strominger, J. L. *J. biol. Chem.* **262,** 16087–16094 (1987).
10. Stern, L. J. & Wiley, D. C. *Cell* **68,** 465–477 (1992).
11. Bjorkman, P. J. *et al. Nature* **329,** 506–512 (1987).
12. Brown, J. H. *et al. Nature* **332,** 845–850 (1988).
13. Bricogne, G. *Acta crystallogr.* **A32,**832–847 (1976).
14. Sussman, J. L., Holbrook, S. R., Warrant, R. W., Church, G. M. & Kim, S.-H. *J. molec. Biol.* **123,** 607–630 (1978).
15. Falk, K., Rötzschke, O., Stevanovic, S., Jung, G. & Rammensee, H.-G. *Nature* **351,** 290–296 (1991).
16. Gorga, J. C. *Crit. Rev. Immun.* **11,** 305–335 (1992).
17. Madden, D. R., Gorga, J. C., Strominger, J. L. & Wiley, D. C. *Cell* **70,** 1035–1048 (1992).
18. Silver, M. L., Guo, H.-C., Strominger, J. L. & Wiley, D. C. *Nature* **360,** 367–369 (1992).
19. Fremont, D. H., Matsumura, M., Stura, E. A., Peterson, P. A. & Wilson, I. A. *Science* **257,** 919–927 (1992).
20. Bjorkman, P. J. *et al. Nature* **329,** 512–518 (1987).
21. Griffith, I. J. *et al. J. exp. Med.* **167,** 541–555 (1988).
22. Peccoud, J., Dellabona, P., Allen, P., Benoist, C. & Mathis, D. *EMBO J.* **9,** 4215–4223 (1990).
23. Sette, A. *et al. J. Immun.* **143,** 3289–3294 (1989).
24. Sidney, J. *et al. J. Immun.* **149,** 2634–2640 (1992).
25. Hammer, J., Takacs, B. & Sinigaglia, F. *J. exp. Med.* **176,** 1007–1013 (1992).
26. Geluk, A. *et al. J. Immun.* **149,** 2864–2871 (1992).
27. Racioppi, L., Ronchese, F., Schwartz, R. H. & Germain, R. N. *J. Immun.* **147,** 3718–3727 (1991).
28. Braunstein, N. S. & Germain, R. N. *Proc. natn. Acad. Sci. U.S.A.* **84,** 2921–2925 (1987).
29. Braunstein, N. S., Germain, R. N., Loney, K. & Berkowitz, N. *J. Immun.* **145,** 1635–1645 (1990).
30. Horn, G. T., Bugawan, T. L., Long, C. M. & Erlich, H. A. *Proc. natn. Acad. Sci. U.S.A.* **85,** 6012–6016 (1988).
31. Miyazaki, T. *et al. Nature* **345,** 722–724 (1990).
32. Slattery, R. M. *et al. Nature* **345,** 724–726 (1990).
33. Lund, T. *et al., Nature* **345,** 727–729 (1990).
34. Saper, M. A., Bjorkman, P. J. & Wiley, D. C. *J. molec. Biol.* **219,** 277–319 (1991).
35. Guo, H.-C. *et al. Nature* **360,** 364–388 (1992).
36. Jardetzky, T. S. *et al. EMBO J.* **9,** 1797–1803 (1990).
37. Busch, R., Hill, C. M., Hayball, J. D., Lamb, J. R. & Rothbard, J. B. *J. Immun.* **147,** 1292–1298 (1991).
38. DeMotz S., Barbey, C., Corradin, G., Amoroso, A. & Lanzavecchia, A. *Eur. J. Immun.* **23,** 425–432 (1993).
39. Newton-Nash, D. K. & Eckels, D. D. *J. Immun.* **150,** 1813–1821 (1993).
40. Konig, R., Huang, L.-Y. & Germain, R. N. *Nature* **356,** 796–798 (1992).
41. Cammarota, G. *et al. Nature* **356,** 799–801 (1992).
42. Madden, D. R., Gorga, J. C., Strominger, J. L. & Wiley, D. C. *Nature* **353,** 321–325 (1991).
43. Garrett, T. P. J., Saper, M. A., Bjorkman, P. J., Strominger, J. L. & Wiley, D. C. *Nature* **342,** 692–696 (1989).
44. Krieger, J. I. *et al. J. Immun.* **146,** 2331–2340 (1991).
45. Kropshofer, H., Bohlinger, I., Max, H. & Kalbacher, H. *Biochemistry* **30,** 9177–9187 (1991).
46. Klinman, N. R. *J. exp. Med.* **136,** 241–260 (1972).
47. Janeway, C. A. Jr *et al. Cold Spring Harb. Symp. quant. Biol.* **54,** 657–666 (1989).
48. Koulova, L., Clark, E. A., Shu, G. & DuPont, B. *J. exp. Med.* **173,** 759–762 (1991).
49. Nabavi, N. *et al. Nature* **360,** 266–268 (1992).
50. Schwartz, R. H. *Cell* **71,** 1065–1068 (1992).
51. Watts, T. H., Alaverdi, N., Wade, W. F. & Linsley, P. S. *J. Immun.* **150,** 2192–2202 (1993).
52. DeVos, A. M., Ultsch, M. & Kossiakoff, A. A. *Science* **255,** 306–312 (1992).
53. Kaye, J. & Janoway, C. A. Jr *J. exp. Med.* **159,** 1397–1412 (1984).
54. Roche, P. A., Marks, M. S. & Cresswell, P. *Nature* **354,** 392–394 (1991).
55. Springer, T. A., Kaufman, J. F., Terhorst, C. & Strominger, J. L. *Nature* **268,** 213–218 (1977).
56. Jencks, W. P. *Proc. natn. Acad. Sci. U.S.A.* **78,** 4046–4050 (1981).
57. Glaichenhaus, N., Shastri, N., Littman, D. R. & Turner, J. M. *Cell* **64,** 511–520 (1991).
58. DeMagistris, M. T. *et al. Cell* **68,** 625–634 (1992).
59. Alexander, J. *et al. J. Immun.* **150,** 1-7 (1993).
60. Racioppi, L., Ronchese, F., Matis, L. A. & Germain, R. *J. exp. Med.* **177,** 1047–1060 (1993).
61. Matsui, K., *et al., Science* **254,** 1788–1791 (1991).
62. Harrison, S. C. *J. Appl. Crystallogr.* **1,** 84–89 (1968)
63. Blum, M. Metcalf, P., Harrison, S. C. & Wiley, D. C. *J. appl. Crystallogr.* **20,** 235–242 (1987).
64. Stuart, D. & Artymiuk, P. *Acta crystallogr.* **A40,** 713–716 (1984).
65. Teng, T.-Y. *J. Appl. Crystallogr.* **23,** 387-391 (1990).
66. Hodel, A., Kim, S.-H. & Brünger, A. T. *Acta crystallogr.* **A48,** 851–858 (1992).
67. Jones, T. A. *J. Appl. Crystallogr.* **11,** 268–272 (1978).
68. Colman, P. M. *Adv. Immun.* **43,** 99–132 (1988).
69. Kwong, P. D. *et al. Proc. natn. Acad. Sci. U.S.A.* **87,** 6423–6427 (1990).

ACKNOWLEDGEMENTS. We thank P. Klimovitsky, A. Haykov and M. Frayser for technical assistance; K. Svenson, assisted by M. Pietras, for the large-scale production of tissue culture cells; and other members of our group and the CHESS synchrotron staff for assistance with X-ray data collection. We acknowledge conversations with R. Germain who reached similar conclusions about how a dimer might not preexist, but only be stabilized by TCR binding. J.H.B. is supported by the Howard Hughes Medical Institute, T.S.J. by the Cancer Research Institute; J.C.G. by the Juvenile Diabetes Foundation International. L.J.S. by a Damon Runyon–Walter Winchell Cancer Fellowship and the Howard Hughes Medical Institute; R.G.U. by the Irvington Institute; J.L.S. by the NIH. D.C.W. is an Investigator with the Howard Hughes Medical Institute. Preliminary, unrefined coordinates of DR1 are available from the authors.